JOURNAL OF MATERIALS SCIENCE 30 (1995) 5799–5807

The effect of nitrogen on the structure and mobility of dislocations in Fe–Ni–Cr austenite

M. GRUJICIC
Center for Advanced Manufacturing, Department of Mechanical Engineering, Clemson University, Clemson, SC 29634, USA

The structure and the critical resolved shear stress for the motion of the straight $a/2\langle 1\,1\,0\rangle$ edge and screw dislocations in Fe–Ni–Cr and Fe–Ni–Cr–N austenite have been analysed using the conjugate gradient method to minimize the potential energy of the crystal and the embedded atom method to quantify atomic interactions at 0 K. In Fe–Ni–Cr austenite both the edge and the screw dislocations dissociate along one of the $\{1\,1\,1\}$ planes forming a stacking-fault ribbon. The ribbon widths are comparable to their values calculated using continuum theory. Dissociated edge and screw dislocations require very similar levels of shear stress for their motion. In Fe–Ni–Cr–N austenite, the structure of the dislocation core of the $a/2\langle 1\,1\,0\rangle$ edge dislocation does not seem to be significantly affected by the presence of nitrogen. In sharp contrast, the core structure of the dissociated $a/2\langle 1\,1\,0\rangle$ dislocation undergoes a major change, resulting in spreading of the core on to two or more non-parallel planes. As a result, a significantly higher level of stress is required for the motion of a screw than an edge dislocation. Under certain conditions the interaction of nitrogen atoms with screw dislocations can result in pinning of the dislocations. The potential mechanism for the motion of the pinned screw dislocations by formation and motion of edge-type kinks is briefly discussed.

1. Introduction

It is well established [1, 2], that addition of nitrogen into Fe–Ni–Cr austenite causes dislocations to become predominantly screw type. In addition, Fe–Ni–Cr–N alloys show an "unusually" high temperature dependence of flow stress at lower temperatures [3]. These characteristics, the predominance of screw dislocations and the rapid increase in flow stress with decreasing temperature, are typically found in bcc alloys, not fcc alloys like austenite (e.g. [4]). The behaviour of bcc alloys is rationalized in terms of lower mobility of screw dislocations, which is caused by a non-planar sessile configuration of their core [4–6]. Recently, the presence of nitrogen in Fe–Ni–Cr austenite was also reported to cause non-planar dissociation of the $a/2\langle 1\,1\,0\rangle$ screw dislocations [7]. In the present paper, the effect of nitrogen on the core structure and relative mobility of the $a/2\langle 1\,1\,0\rangle$ edge and screw dislocation in Fe–Ni–Cr alloys is examined using atomistic simulation. All the simulations were done at 0 K using the conjugate gradient method [8] to minimize the potential energy of the crystal with respect to atoms positions. The use of the conjugate gradient method in the atomistic simulations of the dislocation core structure has been recently reviewed [7] and will not be repeated here.

2. Embedded-atom method

The embedded-atom method (EAM) was originally developed by Daw and Baskes [9, 10], and its theory and application have recently been reviewed [11]. In the EAM the potential energy, E_{pot}, of a system containing N atoms is defined as

$$E_{\text{pot}} = \sum_{i=1}^{N} F_i(\rho_i) + \sum_{\substack{i<j \\ i,j=1}}^{N} \phi_{ij}(r_{ij}) \quad (1)$$

where $F_i(\rho_i)$ is the energy to embed an atom in the electron density, ρ_i, at the location of atom i, and $\phi_{ij}(r_{ij})$ is the two-body Coulombic interaction potential between atoms i and j separated by a distance r_{ij}. The electron density, ρ_i, at the location of atom i is given by a linear superposition of spherically averaged atomic densities of all other atoms in the system, ρ_j^{α} as follows

$$\rho_i = \sum_{\substack{j=1 \\ j\neq i}} \rho_j^{\alpha}(r_{ij}) \quad (2)$$

The atomic densities are generally determined using the Hartree–Fock theory and double-zeta electron density functions as tabulated by Clementi and Roetti [12].

The $\phi_{ij}(r_{ij})$ potential is typically represented as

$$\phi_{ij}(r_{ij}) = Z_i(r_{ij}) Z_j(r_{ij})/r_{ij} \quad (3)$$

where Z_i and Z_j are, respectively, the effective charge functions for atoms i and j which are positive quantities which decrease monotonically with the interatomic distance r_{ij}.

Using experimental data for the cubic elastic constants, the cohesion energies, the equilibrium lattice

0022–2461

parameters, and the heats of mixing in the limit of infinite dilution, Grujicic and Zhou [11] recently determined the $F_i(\rho_i)$, $\rho(r_{ij})$ and $\phi_{ij}(r_{ij})$ functions for iron, nickel, chromium and nitrogen in the Fe–Ni–Cr–N austenitic steels. These functions have been utilized in the present paper to quantify atomic interactions in the computational crystal used in computer simulations.

Our preliminary results showed that the structure of the dislocation core in the Fe–Ni–Cr austenite is somewhat affected by the local chemical composition and the atomic order. In order to eliminate this effect and determine the general influence of nitrogen on the dislocation core structure we applied the effective atom method, in which the metallic sublattice in the austenite is regarded as an aggregate of identical (effective) metallic atoms [11, 13]. The embedding energy and the electron density functions for the effective (metallic) atoms are defined as a weighted average of the corresponding functions for iron, nickel and chromium

$$F_{\text{eff}}(\rho) = \sum_{i=\text{Fe,Ni,Cr}} y_i F_i(\rho) \tag{4}$$

$$\rho_{\text{eff}}(r) = \sum_{i=\text{Fe,Ni,Cr}} y_i \rho_i(r) \tag{5}$$

The effective pair potential function is defined as a weighted average of the pair potentials between iron, nickel and chromium and their "average" neighbours. That is

$$\phi_{\text{eff}}(r) = \sum_{i=\text{Fe,Ni,Cr}} y_i \phi_{i\alpha}(r) \tag{6}$$

where

$$\phi_{i\alpha}(r) = \sum_{j=\text{Fe,Ni,Cr}} y_j \phi_{ij}(r) \qquad \text{for } i = \text{Fe, Ni, Cr} \tag{7}$$

Substitution of Equation 7 into Equation 6 yields

$$\phi_{\text{eff}}(r) \sum_{i=\text{Fe,Ni,Cr}} \sum_{j=\text{Fe,Ni,Cr}} (2-\delta_{ij}) y_i y_j \phi_{ij}(r) \tag{8}$$

where δ_{ij} is the Kroenecker delta function and y is the metal site fraction.

Based on Equations 3 and 8, the effective charge function for the effective atoms is

$$Z_{\text{eff}}(r) = \sum_{i=\text{Fe,Ni,Cr}} \sum_{j=\text{Fe,Ni,Cr}} (2-\delta_{ij}) y_i y_j Z_i(r) Z_j(r) \tag{9}$$

Using Equations 4, 5, 8 and 9 and the $F_i(\rho_i)$, $\rho_i(r)$, $\phi_{ij}(r)$ and $Z_{ij}(r)$ functions for iron, nickel and chromium from our previous work [11], the effective functions $F_{\text{eff}}(\rho)$, $\rho_{\text{eff}}(r)$, $\phi_{\text{eff}}(r)$ and $Z_{\text{eff}}(r)$ were determined.

To avoid surface effects and simulate the behaviour of an infinite dislocation, periodic boundary conditions were applied in the direction parallel to the dislocation line. When nitrogen is introduced into the computational crystal to study its effect on the dislocation structure due to periodic boundary conditions, nitrogen atoms form an infinite string of atoms parallel to the dislocation line, and hence, there is an unrealistically high (line) concentration of nitrogen. To overcome this problem, the periodic length of the computational crystal in the dislocation line direction has to be increased by a large factor, making the size of the computational crystal prohibitively large and the computation impractical. It must be noted that because an unphysically large concentration of nitrogen atoms was used in the present study, the results obtained could be used only for a qualitative analysis of the effect of nitrogen.

3. Computational procedure

3.1. Computational crystal and dislocation generation

3.1.1. Edge dislocation

A rectangular computational crystal containing initially 5148 atomic sites arranged on two interpenetrating fcc lattices was used in the analysis of the edge $a/2\langle 1\,1\,0\rangle$ dislocation. The orientation and the size of the crystal are given in Fig. 1. The edge sizes are expressed in terms of the number of non-equivalent $(\bar{2}\,2\,0)$, $(1\,1\,1)$ and $(1\,1\,\bar{2})$ planes in either of the two sublattices. Initially, equivalent (metallic) atoms were placed on to one of the fcc lattices and the potential energy of the crystal minimized under the conditions of flexible periodic conditions along all three principal directions. This procedure yielded the equilibrium lattice parameters at 0 K. All the subsequent calculations were done under the condition that the lattice parameter remains fixed.

To generate an $a/2[\bar{1}\,1\,0]$ edge dislocation, two neighbouring $[\bar{2}\,2\,0]$ half-planes were removed from the bottom half of the crystal. This procedure reduced the total number of lattice sites to 5172. To help the resulting edge dislocation dissociate into two Shockley partial dislocations, one of the adjacent $(\bar{2}\,2\,0)$ half-planes was shifted into the position of one of the "missing" half-planes, Fig. 1. This resulted in a one-plane separation of the two missing (or extra) $(2\,2\,0)$ planes. Minimization of the potential energy of this configuration, causes further separation of the two extra half-planes, i.e. further separation of the two Shockley partial dislocations. All the calculations were done under the periodic boundary condition in the $[1\,1\,\bar{2}]$ direction and free-surface boundary conditions in the $[\bar{1}\,1\,0]$ and $[1\,1\,1]$ directions and hence

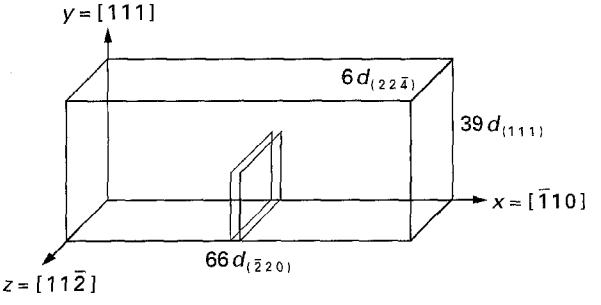

Figure 1 Geometry and size of the computational crystal used in the analysis of the $a/2[\bar{1}\,1\,0]$ edge dislocation. Two $(\bar{2}\,2\,0)$ half-planes indicated in the figure were removed in order to generate the edge dislocation.

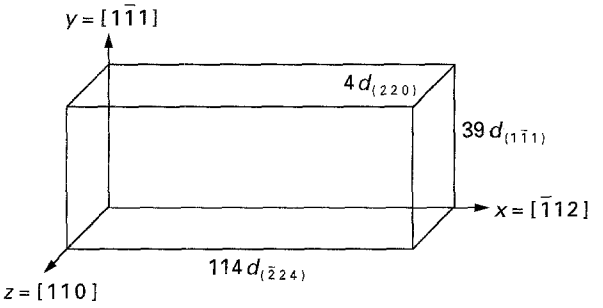

Figure 2 Geometry and size of the computational crystal used in the analysis of the $a/2[1\,1\,0]$ screw dislocation.

pertain to the case of a single infinitely long edge dislocation.

3.1.2. Screw dislocation

The geometry and the size of the computational block used in the analysis of the $a/2\langle 1\,1\,0\rangle$ screw dislocation is shown in Fig. 2. The block contained 5320 atomic sites arranged on two interpenetrating fcc lattices. The size of the computational crystal is again given in terms of the number of non-equivalent $(\bar{2}\,2\,4)$ $(\bar{1}\,1\,1)$ and $(2\,2\,0)$ planes. Using the aforementioned procedure, the equilibrium lattice parameter at 0 K was obtained again. As expected, the same value for the lattice parameter ($a = 0.3578$ nm) was obtained for both computational crystals. The lattice parameter was fixed at this value in all subsequent calculations.

To generate a screw dislocation along the $[1\,1\,0]$ direction, atoms were displaced from their perfect positions (x, y) in the $[1\,1\,0]$ direction according to the formula

$$w = \frac{\boldsymbol{b}}{2\pi} \arctan \frac{y - y_0}{x - x_0} \tag{10}$$

where $\boldsymbol{b}$ is the magnitude of the Burgers vector, and (x_0, y_0) the coordinates of the dislocation centre. In our previous work [7] we explored the effect of various elastic centres of the dislocation on its energy and found that the dislocation centre (marked Δ in Fig. 6a below) is associated with the lowest energy. Hence only this screw dislocation configuration was analysed in the present paper. As discussed elsewhere [7], to initiate dissociation of the unit $a/2[1\,1\,0]$ screw dislocation, periodic boundary conditions were initially applied along all three principal directions in Fig. 2, and the potential energy of the crystal minimized. Free surface-boundary conditions were next applied along the two directions ($[\bar{1}\,1\,2]$ and $[1\,\bar{1}\,1]$) normal to the dislocation line and the energy minimization procedure repeated. This yielded a minor change in the energy and no apparent change in the stacking-fault ribbon width. All the subsequent calculations were carried out under the periodic boundary condition in the $[1\,1\,0]$ direction and free-surface conditions in the other two principal directions and thus pertain to the case of a single, infinitely long dislocation.

3.2. Determination of the critical resolved shear stress

The potential energy minimization technique was also used to determine the critical resolved shear stress for the motion of a straight edge or a screw dislocation. Toward that end, a homogeneous simple shear parallel to the slip plane and in the direction of the Burgers vector of the (undissociated) edge or screw dislocations was applied to the crystal containing the respective type of dissociated dislocation. According to Figs 1 and 2, the corresponding shear stress is τ_{xy} and τ_{zy} for the edge and screw dislocations, respectively. To determine the stress required for the motion of the dislocation, the procedure originally developed by Basinski *et al.* [6] and Duesbery *et al.* [4] was utilized. In this procedure, atoms within the surface layers parallel to the dislocation line are kept fixed at their positions obtained after the application of the shear stress, while the energy of the crystal is being minimized with respect to the positions of interior atoms. After the desired convergence was achieved, the constraints were removed from the surface atoms and the minimization procedure repeated. If the resulting configuration did not involve any motion of the dislocation as a whole, the homogeneous stress was incremented and the aforementioned procedure repeated. This allowed determination of the critical resolved shear stress required to move a straight $a/2\langle 1\,1\,0\rangle$ (edge or screw) dislocation at 0 K.

3.3. Analysis of dislocation core

3.3.1. Edge dislocation

According to Fig. 1, the line direction of the $a/2[\bar{1}\,1\,0]$ edge dislocation is $[1\,1\,\bar{2}]$. To analyse the dislocation core it is convenient to use a projection of the atoms on the plane normal to the dislocation line, the $(1\,1\,\bar{2})$ plane in this case. A $(1\,1\,2)$ projection of the atoms in the fcc structure is given in Fig. 3a. It should be noted that there are six non-equivalent $(2\,2\,\bar{4})$ planes projected in Fig. 3a. However, the analysis carried out here did not entail the use of separate symbols to discriminate between atoms belonging to different non-equivalent $(2\,2\,\bar{4})$ planes.

To display the structure of the dissociated edge dislocation core, edge-type and screw-type relative atomic displacements were determined and shown separately. The edge-type relative displacement of the two atoms is represented by a vector centred at the midpoint of the two atoms, and having the length proportional to the magnitude of the $(1\,1\,\bar{2})$ projection of the relative displacement vector of the two atoms. The arrow on the edge-type relative displacement vector refers to the direction of the edge-type relative displacement of the atom with a larger value of its y coordinate. If the y coordinates of the two atoms are the same, then the arrow refers to the displacement of the atom with a larger x coordinate.

The screw-type relative displacement is represented by a vector centred at the midpoint and lying along the line connecting the two atoms. Its magnitude is proportional to the relative $[1\,1\,\bar{2}]$ displacement of the

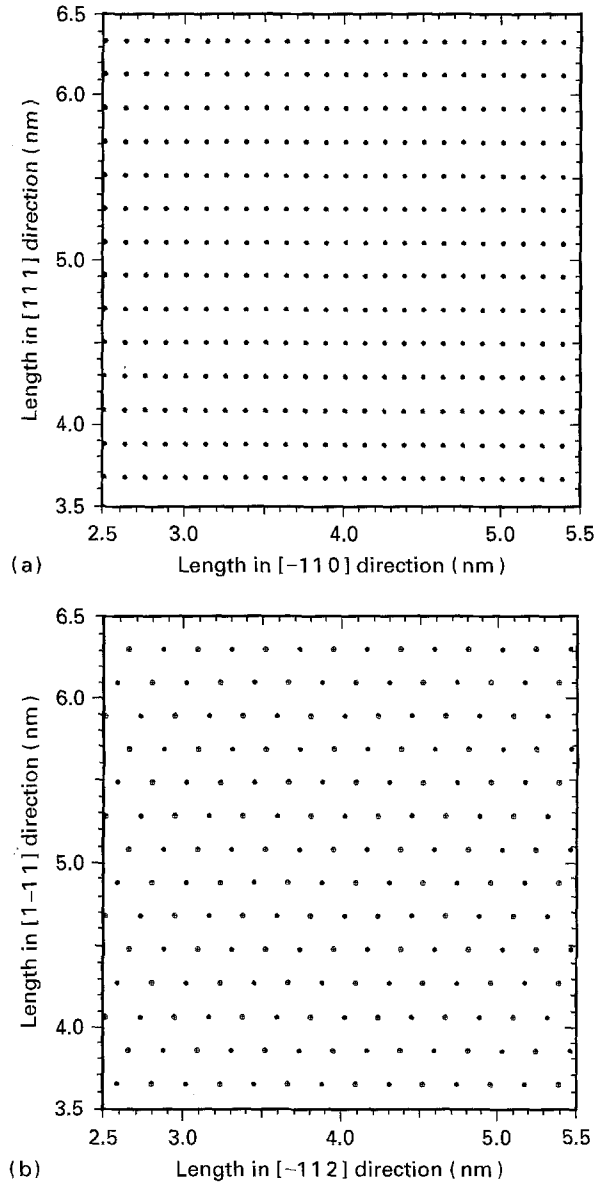

Figure 3 (a) (1 1 $\bar{2}$) projection, and (b) (1 1 0) projection of atoms in the f c c crystal.

two atoms and the arrow points to the atoms whose relative displacement is in the positive [1 1 $\bar{2}$] direction.

Determination of the relative displacements associated with an edge dislocation must be done very carefully since the number of atoms above and below the slip plane is not the same. In the present paper the following procedure was used. The relative differential displacements are determined starting in the region far away from the dislocation, (i.e. at the left side of the computational crystal) where the crystal is nearly perfect and hence the relative displacement are negligible, Fig. 4a and b. As one moves toward the dislocation, the magnitude of the relative displacements increases. When the magnitude of the edge-type relative displacement becomes equal to $\boldsymbol{b}/2 = |a/4[\bar{1}\,1\,0]|$, one skips over two [$\bar{2}$ 2 0] extra halfplanes while calculating the displacements of the atoms above the slip plane relative to the atoms below the slip plane. Since the screw-type relative displacement vectors lie along the line connecting the two atoms in question, the procedure described above can be easily understood with the help of Fig. 4b.

3.3.2. Screw dislocations

To analyse the structure of the dissociated screw dislocation core it is again convenient to use an atomic projection on the plane normal to the dislocation line, the (1 1 0) plane in this case. A (1 1 0) projection of the atoms is given in Fig. 3b, where two different circles were used to distinguish the atoms belonging to two nonequivalent (2 2 0) planes.

The edge-type relative displacements were defined in the same way as in the case of a dissociated edge dislocation. However, the procedure was somewhat simpler to implement in this case since the number of atoms below and above the slip plane was the same. In addition, the edge-type relative displacements were scaled relative to the magnitude of the edge component of the Burgers vector of a Shockley partial, $|a/4[\bar{1}\,1\,2]|$ in this case.

The screw-type relative displacements were defined in the same fashion as in the case of a dissociated edge dislocation. However, they are scaled in this case so that when their magnitude is $\boldsymbol{b}/2 = |a/4[1\,1\,0]|$, the screw-type relative displacement vector just touches the two atoms. When the relative displacement exceeds $\boldsymbol{b}/2$, due to crystal periodicity, it is convenient to have the arrow point towards the other atom.

4. Results and discussion

While the procedure developed here is quite general and can be applied to any Fe–Ni–Cr–N f c c alloy, our calculations were confined to the following two alloys: Fe–40 Ni–15 Cr wt % and Fe–39.90 Ni–14.96 Cr–0.025N wt %. The metal atom site fractions of the two alloys are the same (y_{Fe} =0.4538, y_{Ni} =0.3838 and y_{Cr} =0.1625), while the site fraction of nitrogen is y_N =0.001 in the second alloy. The reason for choosing these two alloys was two-fold: (a) we are currently conducting tensile tests of single crystals of these two alloys at low temperatures and plan ultimately to correlate the experimental data with our atomistic simulation results and, (b) in our previous work [14] we carried out a detailed analysis of the short-range order in the two alloys using Monte Carlo simulations, and hope by gathering various information for the same alloy systems to be able better to elucidate the role of nitrogen in Fe–Ni–Cr austenite.

4.1. Fe–40Ni–15Cr alloy

4.1.1. Edge dislocation

Fig. 4a and b show the equilibrium configuration of the core of the $a/2[\bar{1}\,1\,0]$ edge dislocation in the Fe–40 Ni–15 Cr alloy at 0 K. The dislocation core spreads along the (1 1 1) plane creating a stacking-fault ribbon which is bound with two Shockley partial dislocations. This dislocation dissociation can be represented as follows

$$a/2[\bar{1}\,1\,0] = a/6[\bar{1}\,2\,\bar{1}] + a/6[\bar{2}\,1\,1] \quad (11)$$

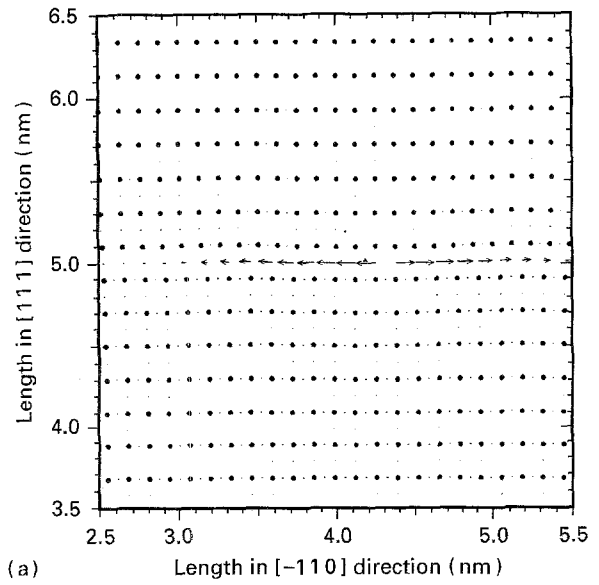

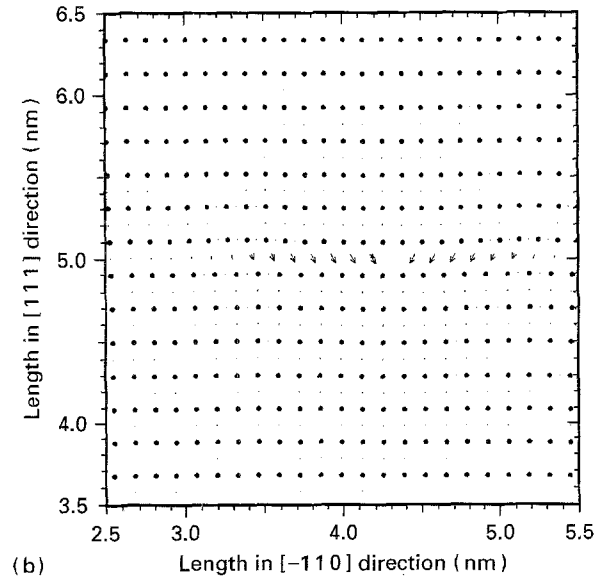

Figure 4 (a) Edge-type, and (b) screw-type relative atomic displacements associated with a dissociated $a/2[1\,1\,0]$ edge dislocation. Fe–Ni–Cr alloy.

The Burgers vector of each of the two Shockley partials, can be represented as a sum of its edge and screw components as follows

$$a/6[\bar{1}\,2\,\bar{1}] = a/4[\bar{1}\,1\,0]_e + 1/12[1\,1\,\bar{2}]_s \quad (12)$$

$$a/6[\bar{2}\,1\,1] = a/4[\bar{1}\,1\,0]_e + 1/12[\bar{1}\,\bar{1}\,2]_s \quad (13)$$

The two partials, thus, differ in the character of the edge component of their Burgers vector. A careful examination of the screw-type relative displacement map, Fig. 4b, shows that the Shockley partial on the left is of the $a/6[\bar{1}\,2\,\bar{1}]$ while the Shockley partial on the right is of the $a/6[\bar{2}\,1\,1]$ type.

The width of the stacking fault ribbon (~ 2 nm) is quite comparable with its value calculated using continuum theory (2.3 nm) and a stacking-fault energy value of 80 mJ m^{-2} [15].

The critical resolved shear stress for the motion of the dissociated $a/2[\bar{1}\,1\,0]$ edge dislocations was found to be close to $0.04G$, where G is the shear modulus for

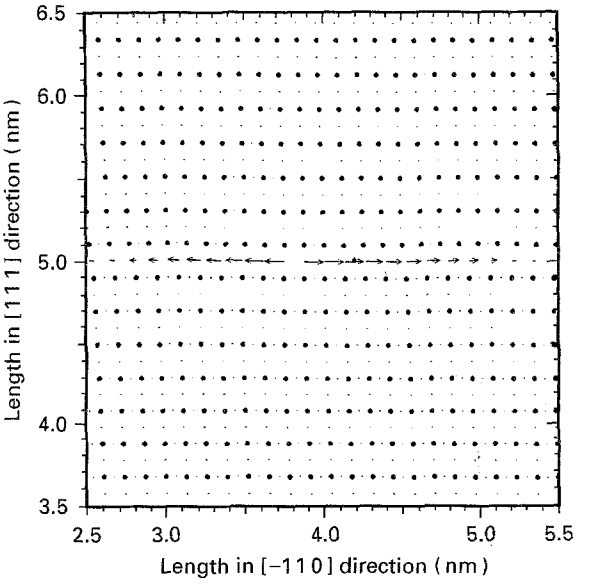

Figure 5 Displaced position of the $a/2[1\,1\,0]$ edge dislocation upon the application of shear stress of $0.04G$, where G is the (1 1 1)-type shear modulus. Fe–Ni–Cr alloy.

the $\{1\,1\,1\}$ planes. Using the value of 65 GPa for the shear modulus G [16], the critical resolved shear stress for the motion of the $a/2\langle 1\,1\,0\rangle$ edge dislocations in the Fe–40 Ni–15 Cr alloy at 0 K was found to be 2600 MPa. Fig. 5 shows the dissociated $a/2[\bar{1}\,1\,0]$ edge dislocation upon the application of shear stress of the above magnitude.

4.1.2. Screw dislocation

Fig. 6a and b show the equilibrium configuration of the core of the $a/2[1\,1\,0]$ screw dislocation in the Fe–40 Ni–15 Cr alloy at 0 K. The dislocation dissociates along the $(1\,\bar{1}\,1)$ plane creating a stacking-fault ribbon which is bound by two Shockley partial dislocations. This process can be represented as

$$a/2[1\,1\,0] = a/6[1\,2\,1] + a/6[2\,1\,\bar{1}] \quad (14)$$

The Burgers vector of each of the two partials can be represented by a sum of its edge and screw components as follows

$$a/6[2\,1\,\bar{1}] = a/4[1\,1\,0]_s + a/12[1\,\bar{1}\,\bar{2}]_e \quad (15)$$

$$a/6[1\,2\,1] = a/4[1\,1\,0]_s + a/12[\bar{1}\,1\,2]_e \quad (16)$$

A careful examination of the edge-type relative displacement map, Fig. 6b, shows that the Shockley partial on the left is of the $a/6[1\,2\,1]$ type and the one on the right of the $a/6[2\,1\,\bar{1}]$ type.

The width of the stacking fault (~ 1.4 nm) is in reasonably good agreement with its value calculated using continuum theory (1.2 nm) and a stacking-fault energy value of 80 mJ m^{-2}.

The critical resolved shear stress for the motion of the dissociated $a/2[1\,1\,0]$ screw dislocation was found to be around $0.04G$ i.e. about 2600 MPa. Fig. 7 shows the dissociated $a/2[1\,1\,0]$ screw dislocation upon the application of shear stress of the aforementioned magnitude.

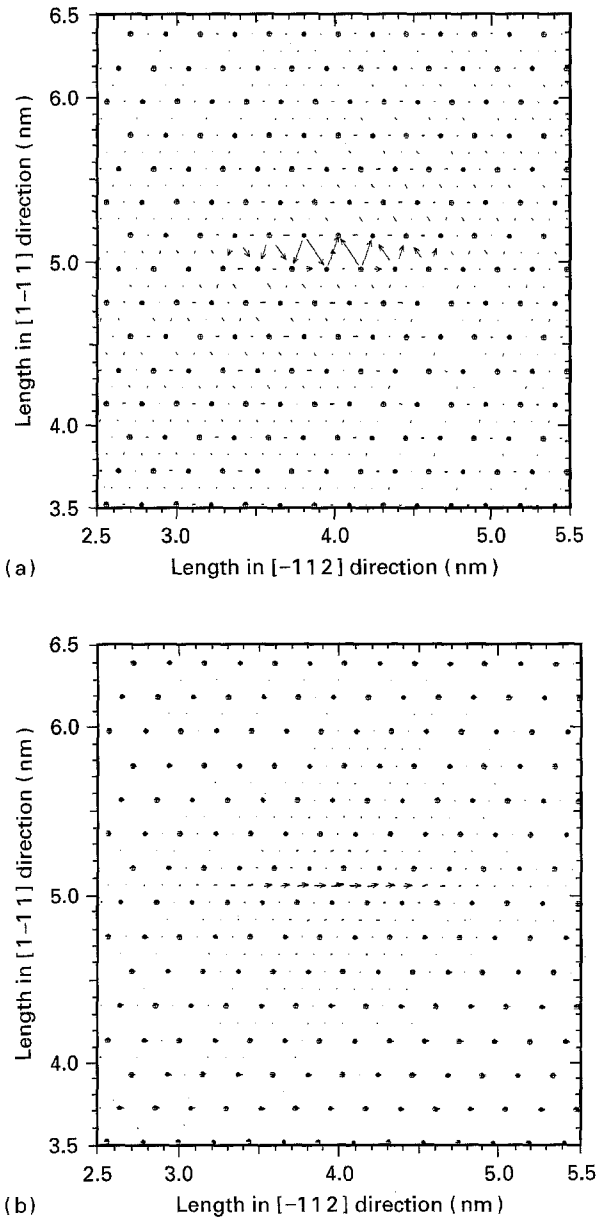

Figure 6 (a) Screw-type, and (b) edge-type relative atomic displacements associated with a dissociated $a/2[1\,1\,0]$ screw dislocation. Fe–Ni–Cr alloy.

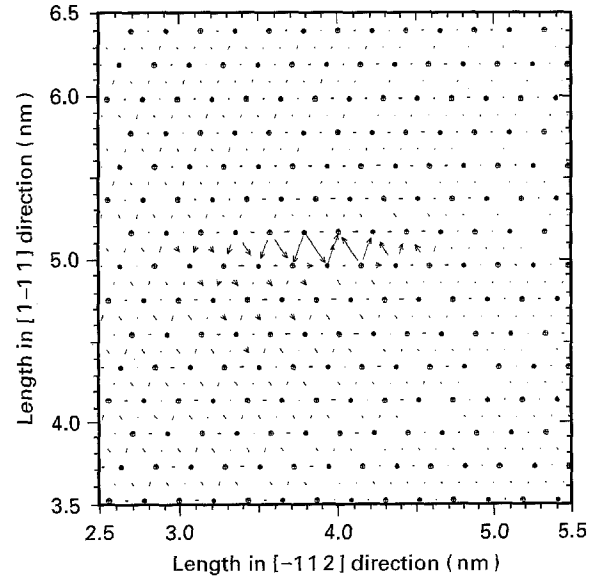

Figure 7 Displaced position of the $a/2[1\,1\,0]$ screw dislocation upon the application of shear stress of $0.04G$. Fe–Ni–Cr alloy.

Based on the findings presented in the section, one can conclude that the mobility, represented here by the critical resolved shear stress for dislocation motion at 0 K, is quite comparable for the straight $a/2\langle 1\,1\,0\rangle$ edge and screw dislocations. It is, hence, understandable that the dislocation substructure in the as-deformed Fe–Ni–Cr alloys generally involves both edge and screw dislocations [2].

4.2. Fe–39.90 Ni–14.96 Cr–0.025N alloy

As demonstrated in our previous work [7], the details of the way nitrogen affects the core structure of the $a/2\langle 1\,1\,0\rangle$ screw dislocations vary with the relative position of the nitrogen atom and the dislocation. However, a particular feature, that is spreading of the dislocation core on to two or more non-parallel planes, was found to be common to all the configurations. For the $a/2\langle 1\,1\,0\rangle$ edge dislocations, we found that the effect of nitrogen on the structure of the dislocation core is much less sensitive to the relative positions of the nitrogen atoms and the dislocation. Therefore, in the present work we compared the effect of nitrogen on the structure of the dislocation core and the critical resolved shear stress for the motion of the two types of dislocations for a fixed relative position of the nitrogen atoms and the dislocation. That is, a row of "equivalent" nitrogen atoms was placed on the slip plane just ahead of the leading Shockley partial dislocation both for the case of a dissociated $a/2[\bar{1}\,1\,0]$ edge dislocation and a dissociated $a/2[1\,1\,0]$ screw dislocation.

4.2.1. Edge dislocation

The effect of nitrogen atoms, placed on the slip plane just ahead of the leading Shockley partial dislocation, on the core structure of the dissociated $a/2[\bar{1}\,1\,0]$ edge dislocation is shown in Fig. 8a and b. Nitrogen causes minor lattice distortions, but does not change the structure of the dislocation core significantly. In particular, no apparent spreading of the dislocation core on to two or more non-parallel planes can be observed. Similar results were obtained when a row of nitrogen atoms was placed above or below the slip plane, and hence will not be shown here.

The critical resolved shear stress for the motion of the dissociated $a/2[1\,1\,0]$ dislocation in the presence of a row of nitrogen atoms on the slip plane just ahead of the leading Shockley partial dislocation was found to be about $0.06G$ i.e. 3900 MPa, Fig. 9. The observed 50% increase in the critical resolved shear stress is about one-half to one-third of the relative increase in the flow stress associated with the addition of 0.025 wt % N into Fe–40 Ni–15 Cr austenite [1, 3].

Based on the findings reported in this section, one can conclude that the interaction of nitrogen atoms with the $a/2\langle 1\,1\,0\rangle$ edge dislocations cannot fully account for the experimentally found strong nitrogen strengthening effect in Fe–Ni–Cr–N austenite. This observation is very important, because in many reports (e.g. [17]), it was speculated that the interstitial

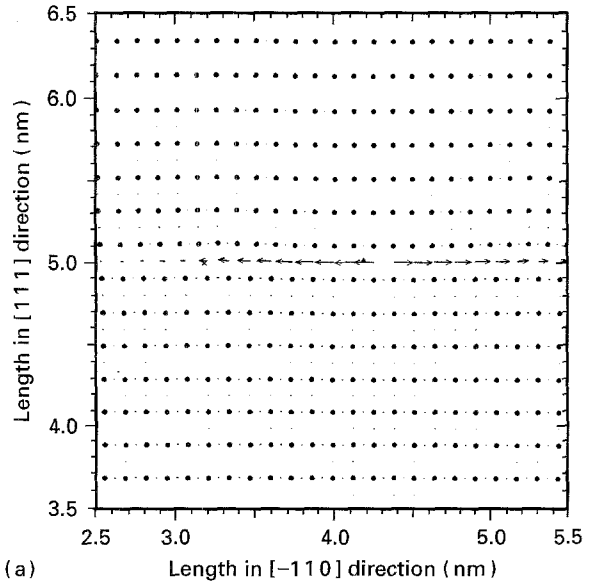

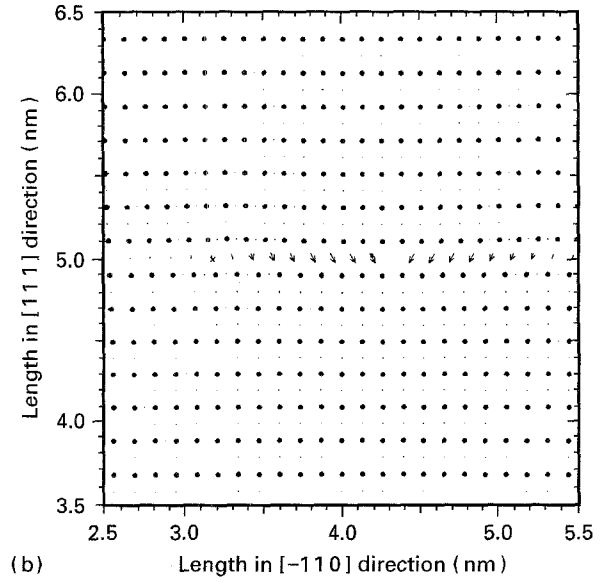

Figure 8 (a) Edge-type, and (b) screw-type relative atomic displacements associated with a dissociated $a/2[\bar{1}10]$ edge dislocation. Fe–Ni–Cr–N alloy.

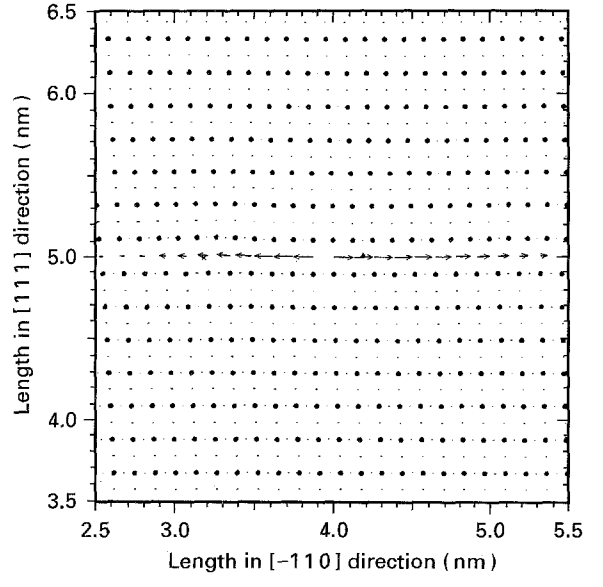

Figure 9 Displaced position of the $a/2[\bar{1}10]$ edge dislocation upon the application of shear stress of $0.06G$. Fe–Ni–Cr–N alloy.

strengthening in fcc alloys of iron is caused by the (dilational) strain interaction between dislocations and nitrogen atoms. Accordingly, the first-order strain interaction between an interstitial and a screw component of a dislocation is zero, and hence only the edge component of a dislocation contributes to interstitial strengthening. Results reported here, however, suggest that the interaction of nitrogen atoms with the edge dislocations does not represent the dominant part of interstitial strengthening, and that the "strain interaction" theory is not very useful in the present case. This is supported by X-ray diffraction measurements [1], which show that nitrogen-induced dilational strains in Fe–Ni–Cr austenite are relatively small and symmetric.

4.2.2. Screw dislocations

The effect of nitrogen atoms, placed on the slip plane just ahead of the leading Shockley partial dislocation,

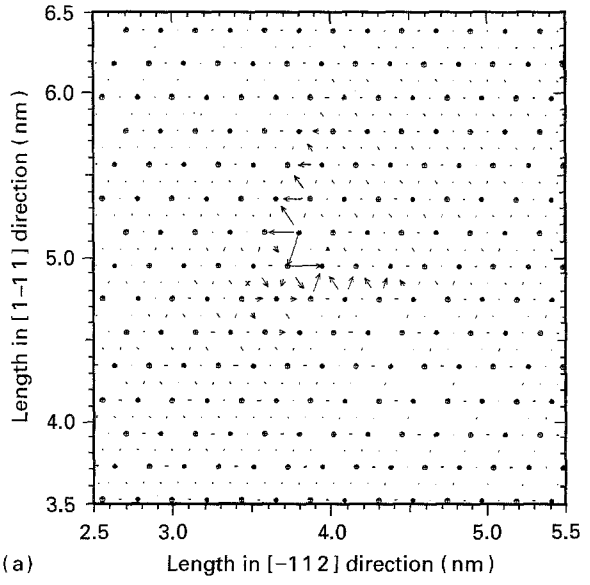

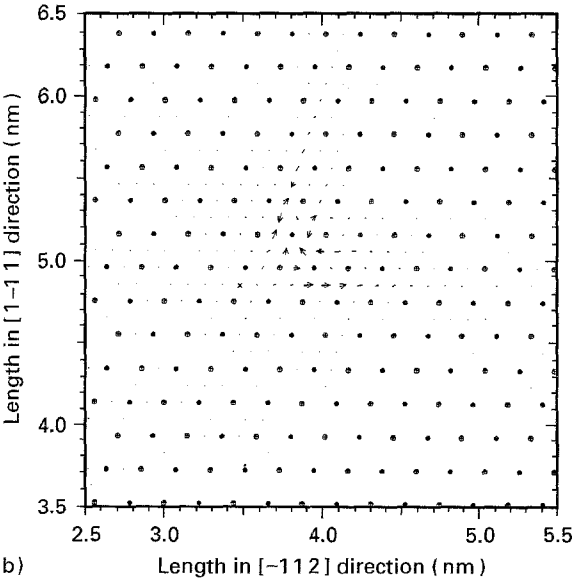

Figure 10 (a) Screw-type, and (b) edge-type relative atomic displacements associated with a dissociated $a/2[1\,1\,0]$ screw dislocation. Fe–Ni–Cr–N alloy.

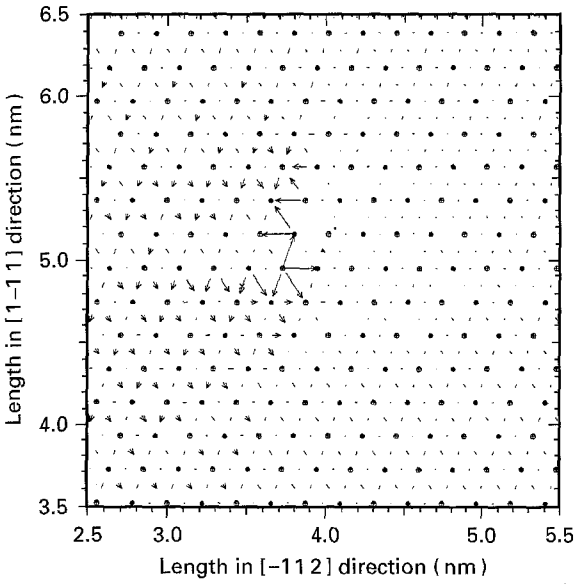

Figure 11 Configuration of the $a/2[1\,1\,0]$ edge dislocation upon the application of shear stress of $0.08G$. Fe–Ni–Cr–N alloy.

on the core structure of the dissociated $a/2[1\,1\,0]$ screw dislocation is shown in Fig. 10a and b. Nitrogen causes spreading of the dislocation core on to two close-packed planes, $(1\,\bar{1}\,1)$ and $(\bar{1}\,1\,1)$. As discussed in our previous work [7], this process can be described as

$$a/2[1\,1\,0] = a/6[1\,2\,1] + a/6[1\,2\,\bar{1}] + a/6[1\,\bar{1}\,0] \quad (17)$$

The last dislocation, $a/6[1\,\bar{1}\,0]$ is of the edge type and its slip plane is $(0\,0\,1)$. Because $(0\,0\,1)$ is not a close-packed plane, glide of the $a/6[1\,\bar{1}\,0]$ dislocation requires a higher stress, and hence the entire dissociated $a/2[1\,1\,0]$ screw dislocation is less mobile.

Determination of the critical resolved shear stress for the motion of the dissociated $a/2[1\,1\,0]$ screw dislocation shown in Fig. 10a and b, turned out to be quite difficult. At a stress level of $0.06G$, the segment of the dislocation residing on the $(1\,\bar{1}\,1)$ plane begins to move to the left, while the segment of the dislocation on the $(\bar{1}\,1\,1)$ plane remains steady. A subsequent increase in stress causes the $(1\,\bar{1}\,1)$ segment to move completely to the left, and subsequently extend in the $[1\,\bar{1}\,\bar{2}]$ direction, Fig. 11. However, the intersection of the two dislocation segments remains sessile. In addition, the entire region around the dislocation becomes distorted. A further increase in stress causes further distortion of the surrounding region but not the motion of the dislocation as a whole.

It appears, hence, that the dissociated $a/2[1\,1\,0]$ screw dislocation is pinned by nitrogen and cannot move as a straight dislocation. However, as pointed out by Duesbery *et al.* [4], the distorted region ahead of the dissociated screw dislocation can assist the formation of edge-type kinks, the latter being of the edge-type require a lower stress for their motion as shown in the previous section and can move laterally causing the screw dislocation to advance. Owing to the use of periodic boundary conditions in the direction of the dislocation, kink formation and motion was not analysed in the present work. Nevertheless, it is clear that nitrogen has a much stronger interaction with the $a/2\langle 1\,1\,0\rangle$ screw dislocations than with the $a/2\langle 1\,1\,0\rangle$ edge dislocations, causing the former to become significantly less mobile than the latter. It is, hence, not surprising that the dislocations in Fe–Ni–Cr–N austenite are predominantly of the screw character.

5. Conclusion

The critical resolved shear stress for the motion of the $a/2\langle 1\,1\,0\rangle$ dislocations is comparable for both edge and screw-type dislocations in Fe–Ni–Cr austenite at 0 K. This explains why both types of dislocation are readily found in these alloys.

The critical resolved shear stress for the motion of the $a/2\langle 1\,1\,0\rangle$ edge dislocation is lower than that for the $a/2\langle 1\,1\,0\rangle$ screw dislocations in Fe–Ni–Cr–N alloys at 0 K. This is in accordance with the TEM observations [2] that dislocations are predominantly of the screw type in Fe–Ni–Cr–N austenite.

For the particular case of the relative position of the nitrogen atoms and the dislocation analysed in this paper, it was found that the $a/2\langle 1\,1\,0\rangle$ screw dislocations become pinned and cannot move as straight dislocations. In such a case, the formation of edge-type kinks and their lateral motion can become the dominant mechanism for the motion of screw dislocations.

Acknowledgements

This work was supported by the National Science Foundation under Grant DMR-9102973. The author is indebted to Dr Bruce MacDonald of NSF for encouragement and continuing interest in the present work. The author thanks Drs M. S. Daw and S. M. Foiles for a number of valuable discussions. The encouragement and friendship of Professor W. S. Owen is greatly appreciated. The help of Mr. X. W. Zhou with the calculations is also acknowledged.

References

1. M. L. G. BYRNES, M. GRUJICIC and W. S. OWEN, *Acta Metall.* **35** (1987) 1853.
2. J. SASSEN, A. J. GARRATT-REED and W. S. OWEN, in "High nitrogen steels, HNS88" (Institute of Metals, London, 1989) p. 1959
3. M. GRUJICIC, J. C. NILSSON, W. S. OWEN and T. THORVALDSSON, *ibid.* p. 151.
4. M. S. DUESBERY, V. VITEK and D. K. BOWEN, *Proc. R. Soc.* **A332** (1973) 85.
5. V. VITEK, R. C. PERRIN and D. K. BOWEN, *Philos. Mag.* **21** (1970) 1049.
6. Z. S. BASINSKI, M. S. DUESBERY and R. TAYLOR, *Can. J. Phys.* **49** (1971) 2160.
7. M. GRUJICIC, *Mater. Sci. Eng.* **A183** (1994) 223.
8. R. FLETCHER and C. M. REEVES, *Computer J.* **7** (1964) 149.
9. M. S. DAW and M. I. BASKES, *Phys. Rev. Lett.* **50** (1983) 1285.

10. *Idem, Phys. Rev.* **B29** (1984) 6443.
11. M. GRUJICIC and X. W. ZHOU, *Calphad* **17** (1993) 383.
12. E. CLEMENTI and C. ROETTI, "Atomic data and nuclear data tables", Vol. 4, nos 3 and 4 (Academic, New York, 1974).
13. R. W. SMITH and G. S. WAS, *Phys. Rev.* **B40** (1989) 10322.
14. M. GRUJICIC and X. W. ZHOU, *Calphad* **17** (1993) 383.
15. A. SEEGER, *Philos. Mag.* **46** (1955) 1194.
16. H. M. LEDBETTER, M. W. AUSTIN and S. A. KIM, *Mater. Sci. Eng.* **85** (1982) 231.
17. R. SANDSTROM and H. BERGQUIST, *Scan. J. Metal.* **6** (1977) 156.

Received 8 February 1994
and accepted 7 June 1995